AIAA JOURNAL
Vol. 38, No. 4, April 2000

Megahertz Pulse-Burst Laser and Visualization of Shock-Wave/Boundary-Layer Interaction

Pingfan Wu,* Walter R. Lempert,† and Richard B. Miles‡
Princeton University, Princeton, New Jersey 08544

The development and application of a Nd:YAG pulse-burst laser system, which is capable of operating at up to 1-MHz pulse repetition rate with high pulse energy and narrow spectral linewidth, is presented. The laser system can generate a burst of from 1 to 99 pulses over a maximum time interval of 100 θs. The average single pulse energy at 1.064θ is 10 mJ. This laser is paired with a new megahertz-rate charge-coupled device framing camera to obtain images of a Mach 2.5 flow over a 14-deg angle wedge at a 500-kHz repetition rate. The sequential images clearly show the dynamic interaction between the incoming turbulent boundary layer and the unsteady oblique shock wave.

I. Introduction

In recent years there has been enormous progress in the development and application of diagnostic imaging techniques, such as planar laser-induced fluorescence (PLIF),[1] Rayleigh scattering,[2] and Raman scattering.[3] However, the ability to capture time-evolving information has been severely constrained by the limitations of laser technology. For example, the pulse repetition rates of commercially available high-energy solid-state lasers are limited up to 30 Hz. Nd:YAG lasers combining continuous pumping with repetitive Q switching at up to 50 kHz have been built.[4] However, the pulse energy at these rates is only about 100 μJ. Also available are 20-kHz repetition-rate metal vapor lasers,[5] with single pulse energy a few millijoules. Newly developed, repetitively Q-switched ruby lasers have pushed the repetition rate up to 500 kHz.[6,7] After amplification the individual pulse energy can get hundreds of millijoules.[7] However, when the repetition rate extends to 1 MHz, repetitive Q-switched operation becomes very unreliable.[6]

Our objective has been to develop a laser imaging system to capture high-speed and unsteady flow phenomena, such as turbulent structure and shock-wave/boundary-layer interactions. The dynamics of the highly unsteady shock-wave/boundary-layer interaction is very important in the stability and control of supersonic vehicle. Because the particular characteristics of the turbulence are still unknown, the dynamic visualization of shock wave and boundary-layer structure becomes very important. The characteristic small-scale eddy turnover time is on the order of microseconds, and so a megahertz repetition-rate laser source and imaging system become critical for this application.

The pulse burst concept is chosen for megahertz rate imaging diagnostics systems because the product of repetition rate and energy per pulse is constrained by the thermal loading that the solid-state lasing elements can tolerate. The current maximum power for a commercially available pulsed Nd:YAG system is approximately 15 W at 1.06 μm (1.5 J/pulse at 10 Hz). This means that, for example, if the megahertz pulse laser were to be run as a continuous duty cycle system, thermal considerations alone would limit the output energy to approximately 150 μJ per pulse. This is approximately 100 times too low to be generally useful for flow imaging experiments. The key to the burst concept is the reduction of the duty cycle in order to achieve high energies in each individual pulse. A typical pulse-burst can be seen in Fig. 1a: every 0.1 s a burst of about 30 pulses is generated (in this figure only 5 pulses are shown).

In this paper we present the design of a Nd:YAG-based, high-power, narrow-linewidth, pulse-burst laser source that can generate a burst of from 1 to 99 laser pulses with an interpulse period as short as 1 μs and a pulsewidth from 10 to 100 ns. The spectral width of these pulses is comparable to the Fourier transform of their temporal profiles, which makes this pulse-burst laser an ideal source for narrow-linewidth, long coherence length applications such as holographic interferometry and filtered Rayleigh scattering (FRS).[8,9] In particular, the FRS is useful for the imaging of high-speed flows because it can be used to suppress background scattering from windows and walls as well as to highlight particular velocity components.

This pulse-burst laser system has been paired with a Princeton Scientific Instruments' fast-framing charge-coupled-device (CCD) camera that can capture up to 30 images at a rate of up to 1 μs a frame. The laser and the camera were set up to visualize the Mach 2.5 flow over a 14-deg wedge from streamwise view and planform view at a 0.5-MHz rate. The optically thick iodine vapor filter was placed in front of the camera and used to highlight different velocity components of the flow by selectively passing different Doppler-shifted frequencies. The images that were acquired clearly illustrate the unsteadiness of the oblique shock wave and show that the unsteady shock motion is closely coupled to the incoming boundary-layer structure.

II. General Description of the Laser

The challenge is to create a controllable pulse-burst system, which produces a uniform set of high-energy pulses with very low background. The background is primarily caused by amplified spontaneous emission that occurs naturally through the amplifier chain. Incidental feedback must also be carefully controlled so that the system does not develop parasitic lasing. In addition, the gain seen by each pulse in the pulse burst is slightly different because of the gain saturation from the previous pulse. In the design of this system, it was decided not to use a regenerative amplifier configuration because of the limited versatility of such a system and concerns regarding gain depletion and Q-switch leakage. The design of the pulse-burst laser system is, therefore, based on a master oscillator power amplifier (MOPA) configuration, as shown in Fig. 2. The laser system consists of six principle parts: 1) monolithic, single-frequency, diode-pumped, CW Nd:YAG laser; 2) four-pass preamplifier 1; 3) pulse slicer (a pair of Pockels cells); 4) two-pass preamplifier 2; 5) three-stage high-energy amplifier chain; and 6) second harmonic crystal.

A continuous wave (CW) Nd:YAG ring laser serves as the master oscillator. The laser can be frequency tuned and has a single mode output. Because this laser is amplified through the amplifier chain,

Received 1 April 1999; revision received 16 August 1999; accepted for publication 18 August 1999.

*Graduate Student, Department of Mechanical and Aerospace Engineering. Student Member AIAA.

†Senior Research Scientist, Department of Mechanical and Aerospace Engineering; currently Associate Professor, Department of Mechanical Engineering, Ohio State University, Columbus, OH 43210.

‡Professor, Department of Mechanical and Aerospace Engineering. Associate Fellow AIAA.

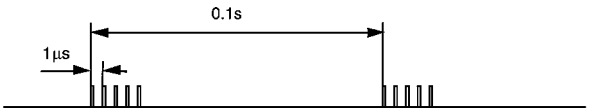

a) CW laser is sliced into pulse-burst, repeated every 0.1 s

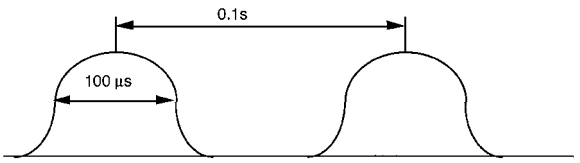

b) Nd:YAG gain curve

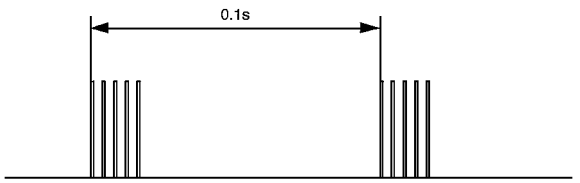

c) Result is high-power "burst" of 1–99 pulses

Fig. 1 Concept of pulse-burst laser system.

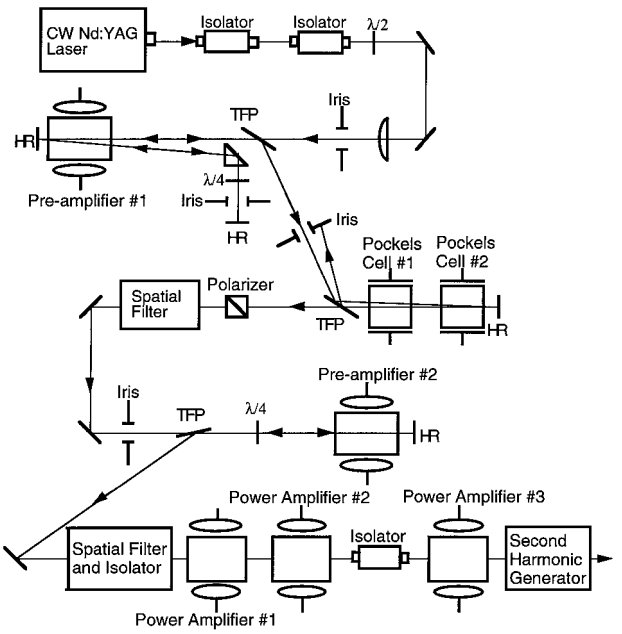

Fig. 2 Schematic diagram of pulse-burst laser system.

its frequency determines the output frequency of the pulse-burst laser system. To minimize amplified spontaneous emission (ASE), the four-pass preamplifier 1 amplifies this CW laser light over the 100-μs-or-so gain window of the flashlamp-pumped Nd:YAG laser rods. The power remains below saturation, and so there is no loss in gain associated with amplifying a CW laser as compared to a pulsed laser in this stage. This CW preamplification suppresses the ASE that would otherwise be present between pulses had the pulse slicing been done before preamplifier 1. ASE occurs continuously during the flashlamp pumping time so that if the light were chopped with a $\frac{1}{100}$ duty cycle the ASE generated in preamplifier 1 would be stronger than the amplified laser signal. This is avoided by putting the pulse slicer after preamplifier 1. The slicer not only chops the pulse but also blocks the cross-talk between preamplifier 1 and preamplifier 2 and, therefore, serves as an isolation stage in the amplifier chain.

III. System Performance

A. Master Oscillator

The master oscillator is a commercially available monolithic Nd:YAG ring laser with output power about 20 mW (Lightwave 120-03A). The frequency of this laser can be voltage-tuned over a range of approximately 1 cm^{-1} at 1.06 μm. The CW laser beam has a very good spectral and spatial profile. The linewidth is about 5 kHz (in 1 ms), and the frequency drift is about 50 MHz/h.

B. Preamplifier 1

Preamplifier 1 is a four-pass, 10-Hz repetition-rate, flashlamp-pumped, 6.5 mm diam × 110 mm long Nd:YAG rod. A long-focal-length (1-m) lens reduces the beam diameter to approximately 2 mm to accommodate the multiple passes. The overall gain of the four-pass system, taking optical losses into account, is approximately 2500 times. Preamplifier 1 is currently operated at much lower level than its maximum gain in order to prevent spontaneous lasing.

C. Pulse Slicer

The pulse slicer, custom built by Medox, Inc. (Ann Arbor, Michigan), consists of a pair of electro-optic Pockels cells, similar to those used as Q switches for standard solid-state laser systems. By applying a suitable voltage, a $\lambda/4$ polarization retardation is imposed upon the laser beam by each Pockels cell for each pass. Consequently, when either one of the cells is on, the resulting polarization is rotated 90 deg (from vertical to horizontal) and is, therefore, transmitted through the thin-film polarizer (TFP). When both (or neither) of the Pockels cells are on, the polarization of the beam is unchanged, and it is reflected by the TFP and blocked by an iris diaphragm.

Figure 3 shows a timing diagram for the pair of Pockels cells. Each individual Pockels cell has a minimum rise time of approximately 4 ns and an on time duration ($t2$) of approximately 150 ns. The delay between the rising edges $t1$ is variable from 5 to 100 ns. The slicer is on, during the interval $t1$ when Pockels cell 1 is high and Pockels cell 2 is low. From the diagram it is apparent that the falling edge is much slower than the rising edge, which is the reason two Pockels cells are used instead of one. For this system the timing of the laser pulses solely depends on the rising edge of the high voltage, which is applied to the Pockels cells. The high-voltage timing is determined by a 500-MHz precision clock that controls the Pockels cells' power supply unit, resulting the timing jitter for the laser pulses that is less than 2 ns. The timing of pulses here is much more precise than the repetitively Q-switched laser,[7] in which even the Q-switched pulse buildup time will cause time uncertainty 10 ns.

D. Preamplifier 2

After the pulse slicer the output pulse train is spatially filtered and then double-passed through preamplifier 2. The spatial filter has two functions: 1) decrease the ASE and 2) clean the spatial profile of the laser.

Preamplifier 2 is an 8 mm diam × 110 mm long Nd:YAG rod. The peak double-pass gain of preamplifier 2 is approximately 13 times. The output peak pulse power is about 650 W, corresponding to an average 13 μJ for a single, 20-ns-duration pulse. Again to prevent

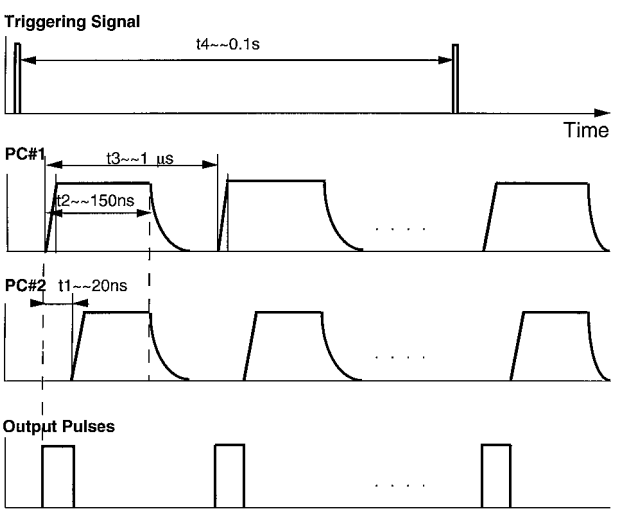

Fig. 3 Timing diagram for the work of the pair of Pockels cells.

spontaneous lasing, preamplifier 2 is operated at a gain level lower than maximum power.

E. Power Amplifier Chain and Second Harmonic Generation

The power amplifier chain consists of three additional Nd:YAG rods, taken from a commercial (Continuum Model YG-592) laser system. The rods are 6.5, 6.5, and 9.5 mm diam, respectively. Between power amplifiers 2 and 3, there are a telescope beam expansion system (not shown in the figure) and a 10-mm-diam optical isolator (Electro-optics Technology, Inc., Traverse City, Michigan). The peak gain of the individual stage has been measured to be 10, 10, and 8 times, respectively, resulting in an overall peak system gain of approximately 2.5×10^7 (including preamplifiers). The corresponding energy is approximately 10 mJ for a single 20-ns duration pulse at 30 pulses per burst.

An important aspect of the system is the saturation of the final power amplifier. For the amplification of a single pulse, Frantz and Nodvik[10] and Lowdermilk and Murry[11] have given the relation

$$E_{\text{out}} = I_{\text{sat}} \times A \times \ell n\left\{1 + \left(\exp\left(\frac{E_{\text{in}}}{I_{\text{sat}} \times A}\right) - 1\right) \times G_0\right\} \quad (1)$$

where E_{in} and E_{out} are, respectively, the input and output energy of the pulse through the amplifier. I_{sat} is called the saturation flux of the amplifier, which is 440 mJ/cm^2 for a Nd:YAG amplifier. A is the area of the cross section of the amplifier. G_0 is the small signal gain of the amplifier, which is defined as

$$G_0 = \exp(g_0 L) = \exp(n\sigma L) \quad (2)$$

where n is the inverted population density and σ is the cross section of the stimulated radiation. L is the length of the rod. We can relate the small signal gain G_0 to the stored energy E_{store}:

$$E_{\text{store}} = nh\nu LA = A \times (h\nu/\sigma) \times \ell n G_0 \quad (3)$$

where h is the Planck constant and ν is the frequency of the laser. For a specific laser amplifier the cross section A and $h\nu/\sigma$ are constant. The small signal gain G_0 is exponentially related to the stored energy E_{store}. In the pulse-burst laser system, as a pulse is being amplified, it depletes the stored energy from the amplifier, and G_0 decreases. From Eq. (1) the pulse amplification ratios decrease from pulse to pulse in the same burst. We have found the overall stored energy in the power amplifiers is about 800 mJ. For a pulse burst with 30 pulses, the first 29 pulses and other losses will take more than 300 mJ from the rods. The gain of the 30th pulse is only about $\frac{1}{8}$ of the gain of the first pulse in the burst. To compensate for this depletion, the preamplifiers are run on the rising edge of the temporal gain curve. This gives an increasing energy per pulse after preamplifier 2 (Fig. 4a), which leads to a more uniform pulse burst after the final amplifier (Fig. 4b). The oscilloscope (Tektronix Model TDS 360) trace was detected by photodiode with 1-ns response time (Thorlabs Model DET210).

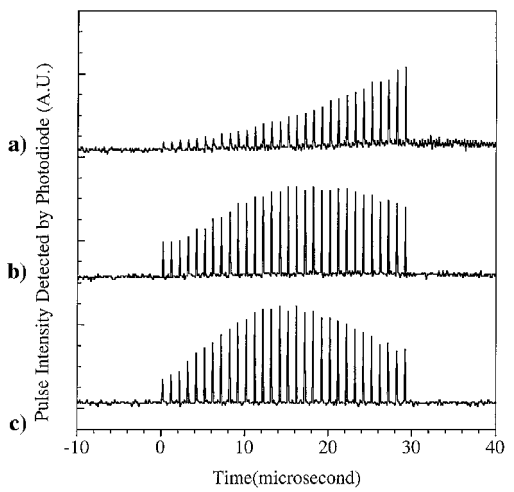

Fig. 4 Single-pulse burst a) before and b) after the final three stages of amplifier train; c) is the second harmonic of the pulse burst. There are 30 pulses per burst, with interpulse separation of 1 θs and single-pulse duration of about 20 ns.

Because of gain depletion, the pulse-to-pulse energy is still far from constant. Especially after doubling, the lowest pulse energy is only about one-third of the highest pulse energy in the same burst. For this reason the dynamic range of the imaging system will decrease by a factor of three, which is still tolerable in our system. With further engineering the nonuniform pulse energy problem can be overcome by using a diode laser to replace the CW Nd:YAG laser as the master oscillator. The diode laser power is easily controlled through the driving current. In that case the input energy of each pulse can be tailored to get a uniform output after the final amplifier.

The final part of the laser system is the second harmonic generator. A telescope system (not shown in the picture) reduces the laser beam diameter to 4 mm before it passes through the doubling crystal. The peak intensity of fundamental light into the doubling crystal is about 4.5 MW/cm^2. The variation in pulse energy is accentuated by the second harmonic process as shown in Fig. 4c. The shape of a single pulse of second harmonic light closely follows that of the fundamental because both are rectangular in time. In contrast to a Gaussian pulse, the temporal profile of the second harmonic of a perfectly rectangular pulse, assuming a simple intensity squared law for conversion efficiency, is identical to that of the fundamental. The full width at half-maximum (FWHM) of the second harmonic is about 14 ns as compared to 16 ns primarily because of the rise time of fundamental pulse. With this system we only get average 0.4 mJ per pulse of second harmonic 0.532 μm. The reason for the low conversion ratio is the low 1.06-μm input intensity. Follow-on work indicates that pulse energy on the order of 25 mJ per pulse at 0.532 μm are achievable with greater amplitude of 1.06-μm light.

IV. Laser Spectral Profile

For many diagnostics applications, narrow spectral linewidth and frequency tunability over a limited range are important. Because the narrow-linewidth CW laser serves as a master oscillator and there is no resonator cavity in the amplification stage, the configuration of the pulse-burst laser system gives a very good spectral profile.

Each individual second harmonic pulse is predicted to have a time-average linewidth on the order of 63 MHz, based on the Fourier transform of a 14-ns rectangular temporal profile ($\delta\upsilon \times \delta t = 0.88$ for a sinc^2/rectangular Fourier transform pair).

As shown in Fig. 5, a 2-GHz free spectral range, confocal Fabry–Perot spectrum analyzer (Burleigh Model RC-46) was used to directly measure the spectral profile of the second harmonic output of the pulse-burst laser. For these measurements the laser was operated at full gain, and the output was attenuated by reflection from an uncoated quartz flat (not shown in Fig. 5). The internal photodiode/mount assembly was removed from the etalon and replaced with a fast response photodiode. The pulsed output from the photodetector was integrated by a boxcar averager (Stanford Research Systems Model SRS 250) and sent to a PC computer. For the data presented next, the boxcar averaged the photodiode voltage over 30 laser shots. Simultaneously, the wavelength of the CW master oscillator was slowly scanned (on the order 1 MHz/s) by applying a computer generated voltage "staircase" (2.5 mV a step) to the input of the laser voltage controller, while holding the voltage to the etalon mirrors constant. The laser, rather than the etalon, was tuned

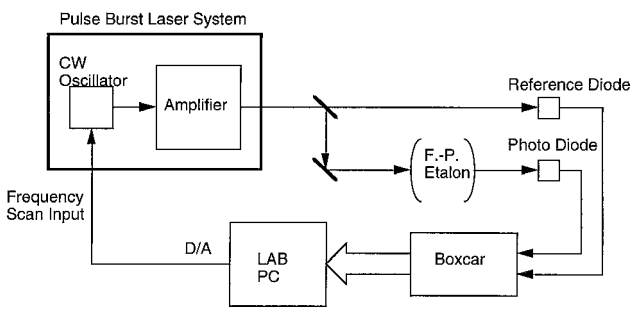

Fig. 5 Schematic diagram for measuring the spectral profile of the pulse-burst laser.

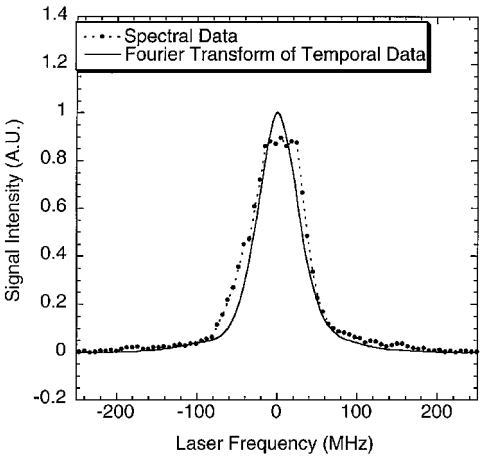

Fig. 6 Time-averaged spectral profile (· · · ·) of second harmonic output of pulse-burst laser and the convolution (——) between the etalon equipment function and Fourier transform of the temporal single-pulse profile.

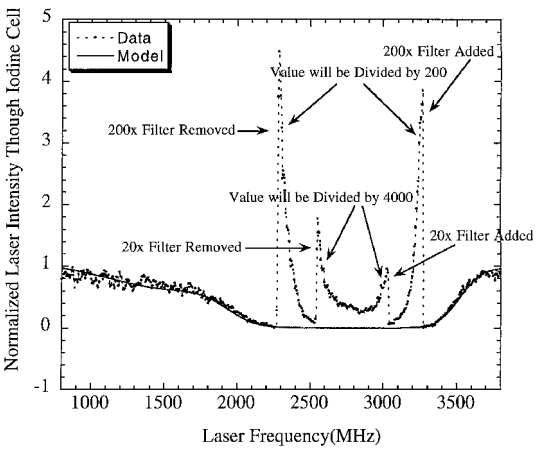

Fig. 7 Experimental attenuation of pulse-burst laser intensity through the iodine cell (· · · ·). Convolution of modeled transmission and laser spectral profile from Fig. 6 (——).

because the etalon could not be scanned slowly enough to capture the profile of the pulsed laser smoothly. The frequency tuning rate of the laser was calibrated with the Fabry–Perot free spectral range. The observed scanning rate was 3 GHz/V and was assumed to be constant over the duration of the scan. The effective finesse of the etalon is measured by passing the CW laser (very narrow linewidth) through the etalon with exactly the same beam path. The measured finesse is about 70, corresponding to spectral resolution of 28 MHz.

Figure 6 (dotted line) shows the measured time-averaged spectral profile of the second harmonic output of the laser, operating nominally with 14-ns duration pulses. Also shown is the convolution between the instrumental function of the etalon and the Fourier transform of a real 14-ns FWHM pulse. It is clear that the spectral profile is approximately the Fourier transform limit of the laser pulse. The Fourier transform of the pulse burst with 30 pulses would be modulated by a high-frequency comb function, but because of the finesse of the etalon, this high frequency cannot be detected.

V. Attenuation of Transmission Through Molecular Iodine Vapor Cell

FRS[8] has the abilities of extracting a weak signal by suppressing background scattering, as well as obtaining quantitative measurements of velocity, temperature, and density of flow simultaneously. The key component of FRS is an optically thick, well-characterized molecular iodine vapor filter that has a very sharp absorption line. The iodine filter, which has been described in detail previously,[9] is 9.98 cm long with cell temperature of 80°C and side-arm temperature at 40°C. The side-arm temperature is maintained to within ±0.1 K with a circulating hot-water bath. In the Rayleigh-scattering experiment, if the frequency of laser source is tuned to the center of the absorption line, the background scattering will be absorbed by the iodine cell while the flowfield signal will pass through the cell because of the Doppler frequency shift. If we tune the laser frequency through the absorption line when measuring the scattered intensity through iodine cell, we can get the spectral shift and the spectral profile of the scattered flow signal and obtain the velocity and temperature of the flow.[8]

Before doing a FRS experiment, it is important to characterize the attenuation of transmission through the iodine cell and the laser spectral purity by scanning the frequency of the laser source through the absorption band. The actual experimental apparatus is similar to Fig. 5, except the Fabry–Perot etalon is replaced by an iodine cell. The second harmonic (0.532-μm) output of the pulse-burst laser hit an aluminum post, and scattered light was collected and passed through the iodine cell. The signal was observed by a photodetector and transferred to the boxcar integrator, as described earlier. At the same time the frequency of the laser was tuned through the absorption lines of iodine. A reference detector was used to monitor the laser output intensity fluctuations as the frequency was tuned. A series of calibrated neutral density filters was used to attenuate the beam prior to tuning into the resonance feature of the iodine

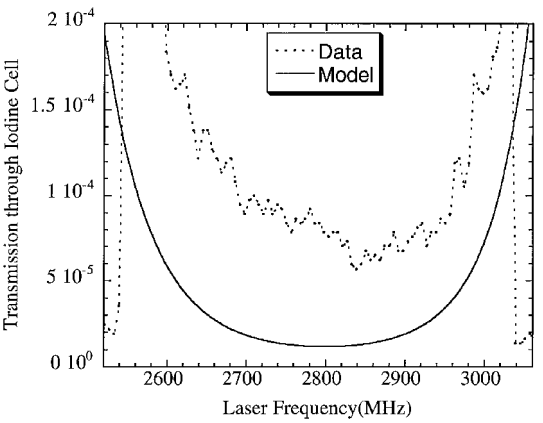

Fig. 8 Blowup of central portion of Fig. 7, illustrating absolute transmission near center iodine absorption line.

vapor. As the laser was tuned into the absorption band, the filters were sequentially removed, boosting the light level reaching the detector. Thus the dynamic range of the attenuation measurement was increased beyond the limitations imposed by the linear operating range of the photodiode.

The dotted line in Fig. 7 shows the experimental result as the frequency was slowly tuned across the absorption line A (around frequency 18788.5 cm^{-1})[9] of the iodine cell. The detected signal has been normalized in such a way as to set the apparent transmission equal to approximately 1 at the endpoints of the scan. When the laser scan passed approximately the 2200-MHz point, a 200-times neutral density filter (Schott Glass Technology, Inc., NG10) was removed from the beam path, resulting in a large increase in signal reaching the detector. Then a second 20-times neutral density filter (Schott NG9) was removed. The neutral density filters were put back as the laser frequency was tuned out of the resonance of iodine. The solid line in Fig. 7 is the convolution between the pulse-burst laser linewidth and the theoretically predicted transmission across the absorption line A. Figure 8 is a blowup of the central 500 MHz of the experimental data (dotted line) and the theoretically predicted transmission (solid line). In this case the experimental data have been converted to absolute transmission by accounting for the attenuation of the neutral density filters. The experimental line center transmission is 5×10^{-5}, as compared to the modeled value of approximately 1.5×10^{-5}. The experimental curve fits well to the theoretical model with a correction for residual transmission. This residual transmission is presumed to arise from the nonideal wings of the laser spectrum and residual ASE. The experiment results not only mean that the pulse-burst laser has very good attenuation when passing through the resonance of the iodine, but the spectral profile of the laser is very good. The laser clearly operates with single mode. These results should be compared to a commercial injection seeded Nd:YAG laser

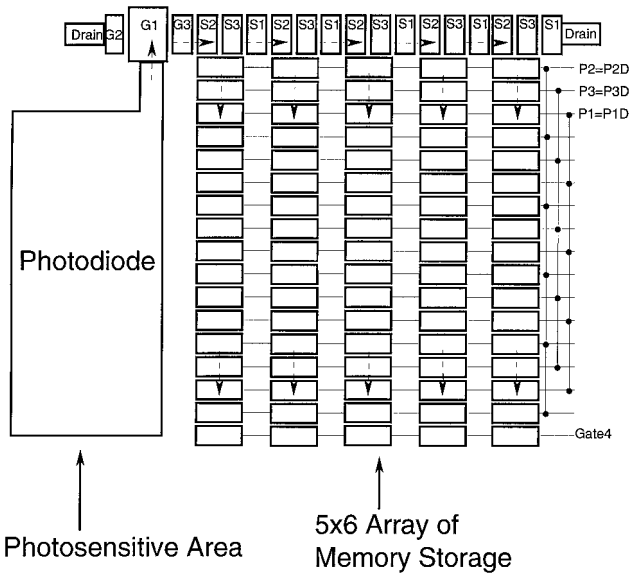

Fig. 9 Architecture of one pixel of megahertz-rate CCD camera. The CCD chip is developed by John Lowrance from Princeton Scientific Instruments, Inc., and Walter Kosonochy from the New Jersey Institute of Technology.

for which the attenuation through iodine resonance only reaches a factor of the order of 300 (Ref. 12), and locking is intermittent.

VI. Fast-Framing Megahertz CCD Camera

A new fast-framing CCD camera[13] developed by Princeton Scientific Instruments, Inc., is used to collect images formed by the pulse-burst laser. The CCD camera chip (U.S. Patent 5355165) has a 30-image storage buffer built into each pixel of the image sensor chip itself and can frame at a rate up to 1 MHz. The pixel format is 360 × 360, divided into four quadrants of 180 × 180 each. A simplified diagram of the architecture of 1 pixel is shown in Fig. 9. Each pixel consists of a photoactive region and a 5 × 6 array of memory elements. The charge is sequentially shifted across the top row of five storage elements at an interval as fast as 1 μs. Subsequently, the charge in each row of memory elements is shifted down in parallel. Upon receipt of a master trigger, the camera operates continuously until a stop trigger is issued. At this point the last 30 images are read out to a standard PC computer.

By coupling the megahertz CCD camera with the pulse-burst laser, a megahertz high-speed flow diagnostic system has been built. This system can capture up to 30 sequential images of rapidly fluctuating phenomena. In the case of high-speed flow, 30 images are usually sufficient to follow the evolution of a structure all the way through the field of view.

VII. Visualization of Shock-Wave/Boundary-Layer Interaction in Mach 2.5 Wind Tunnel

To capture the dynamics of shock-wave/boundary-layer interaction, the pulse-burst laser system has been used to get 0.5-MHz repetition-rate sequential planar images of a turbulent Mach 2.5 boundary flow over a 14-deg wedge.

Figure 10 illustrates the experimental setup to obtain the streamwise view of the dynamics of the turbulent boundary-layer flow. The Mach 2.5 wind tunnel has a cross section of 1 × 0.5 in. The observation region is 16 in. downstream of the throat so that the boundary layer grows to a thickness of about 2 mm. The direction of the flow in the figure is from right to left. To get the streamwise view, a 0.8-mm-wide slit was cut in the centerline of the wedge to let the laser sheet pass through. The size of the slit is small enough to have almost no influence on the overall dynamic process. The second harmonic output of the pulse-burst laser was formed into an approximately 1.5 cm high × 100 μm thick sheet and directed into the flow at an angle of 45 deg with respect to the freestream motion. The angle of 45 deg was chosen to generate enough of a Doppler frequency shift for FRS background suppression. The camera had

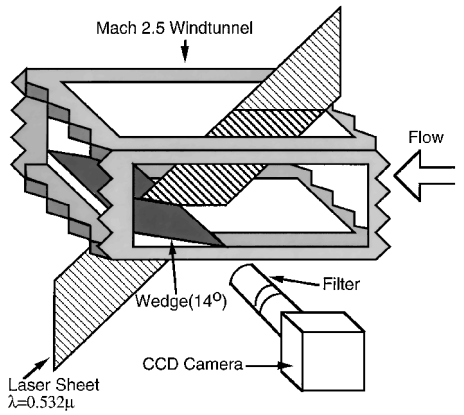

Fig. 10 Experimental setup of side-view visualization of shock-wave/boundary-layer interaction by shooting Mach 2.5 turbulent flow over a 14-deg wedge.

its optical axis perpendicular to the plane of the laser sheet. The flow was run with a stagnation pressure of 120 psig and a stagnation temperature of 258 K. As the Mach 2.5 flow passes by the wedge, an oblique shock forms.

To enhance the scattering signal, gaseous CO_2 was seeded into the flow at a level less than 1% (wt). After the nozzle, because of the temperature decrease of the flow, CO_2 condensed into a finely dispersed fog. We have measured the scattered signal while changing the polarization of incoming laser light. We found the scattering is in the Rayleigh-scattering region so that the condensed CO_2 cluster size is much smaller than the laser wavelength (532 nm). The CO_2 was seeded far upstream in the plenum and was chosen for its ease of handling and because it mixed homogeneously with the air. CO_2 causes less disturbance to the flow than using water vapor as seeder.[14] In the warmer thermal boundary layer the CO_2 is in vapor form, resulting in very high image contrast. The boundary layer is visualized owing to the combined effects of density changes within the boundary layer and CO_2 cluster evaporation. These two effects are related because both result from temperature recovery within the boundary layer. Smith and Smits[15] found the condensed cluster scattering intensity profile in the outer part of a supersonic boundary layer showed good agreement with those obtained using a probe survey.

Figure 11 shows a typical sequence of 25 streamwise view images with an image size of 0.5 × 0.5 in. The time interval between images is 2 μs. The bright straight line at the left bottom corner is the wedge. In particular, comparing images 9 to 15, we can see the curvature of the shock wave has been changed. The unsteady shock-wave motion is coupled with the incoming boundary-layer structure shown in the upstream of shock wave in image 9. The images are conveniently formed into a loop movie to give a dynamic view of the interaction.[§]

The shock-wave/boundary-layer interaction is usually three-dimensional, and so the experiment was also set up to obtain planform view images of the shock-wave/boundary-layer interaction. The layout was similar to that illustrated in Fig. 10 except the laser sheet was parallel to the wall of wind tunnel and grazed the surface of wedge. Figure 12 shows six sequential planform view images each separated by 2 μs. The shock wave now turns into a wavy line, and the boundary-layer structure is seen as the dark region in the flow. From these images it is particularly apparent how the shape of the shock wave changes as the boundary-layer structure passes. A discontinuity in the boundary layer can also be seen as it crosses the shock because the oblique shock changes the direction of the flow, forcing it out toward laser sheet plane.

As the flow crosses the shock, its speed decreases, and the scattered light has a smaller Doppler frequency shift. To highlight the different parts of the flow, we put the molecular iodine vapor cell in front of the camera and tuned the frequency of the laser. With the laser frequency tuned near the center of the iodine absorption, scattering from lower-speed flow and nonmoving elements such as

[§]This movie can be seen on the Web at http://www.princeton.edu/~milesgrp/Movie/PBL1.html.

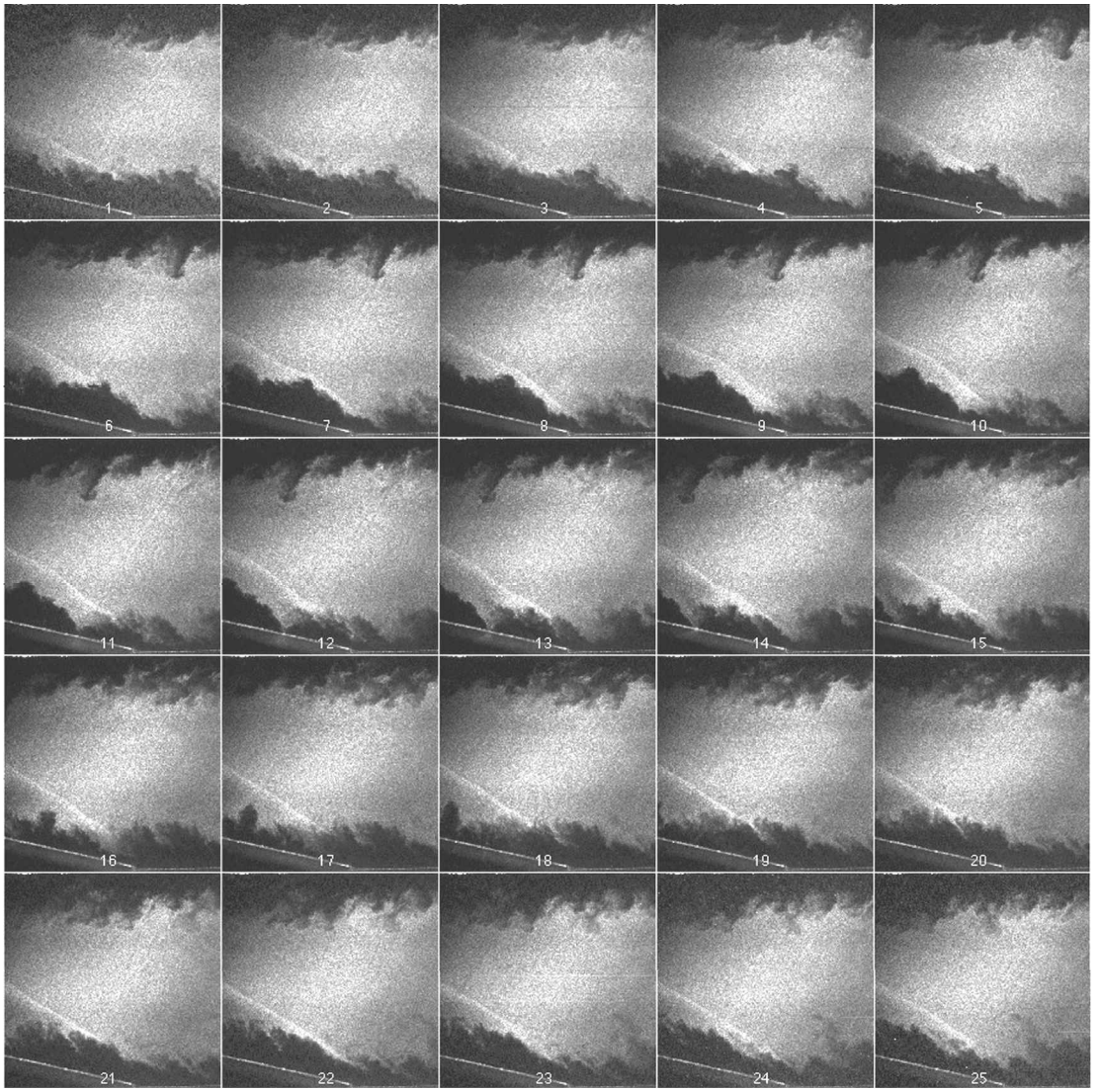

Fig. 11 Sequence of 25 streamwise view images of Mach 2.5 flow over 14-deg wedge. Flow is from right to left with 2 θs between images.

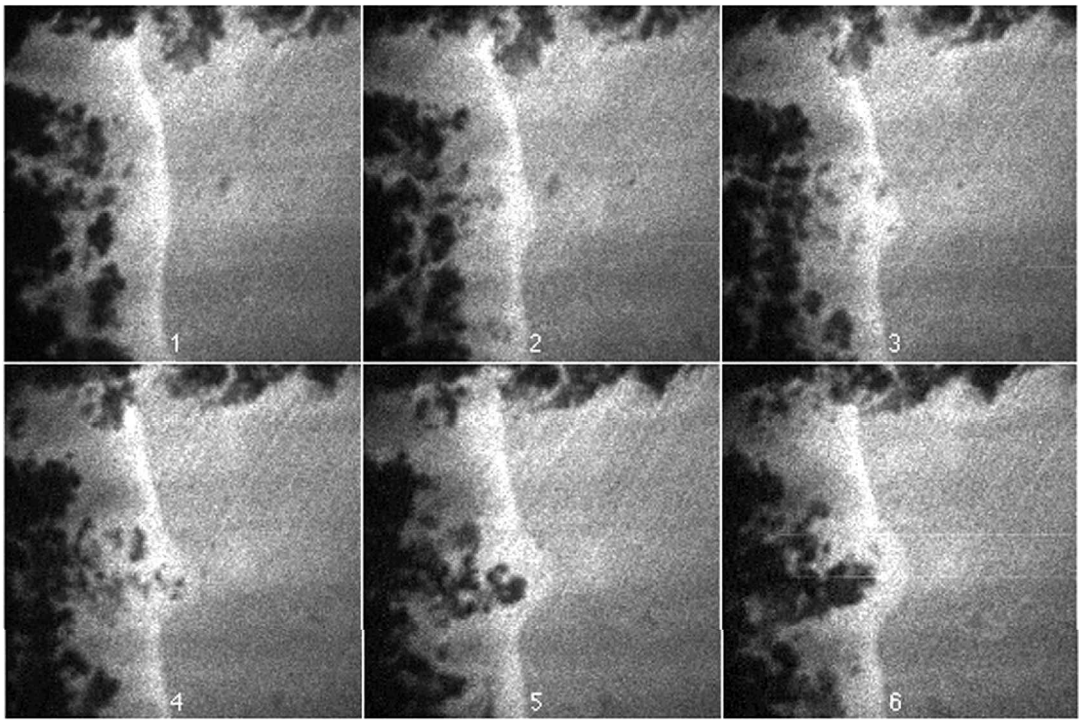

Fig. 12 Sequence of six planform view images of Mach 2.5 flow over 14-deg wedge. Flow is from right to left with 2 θs between images.

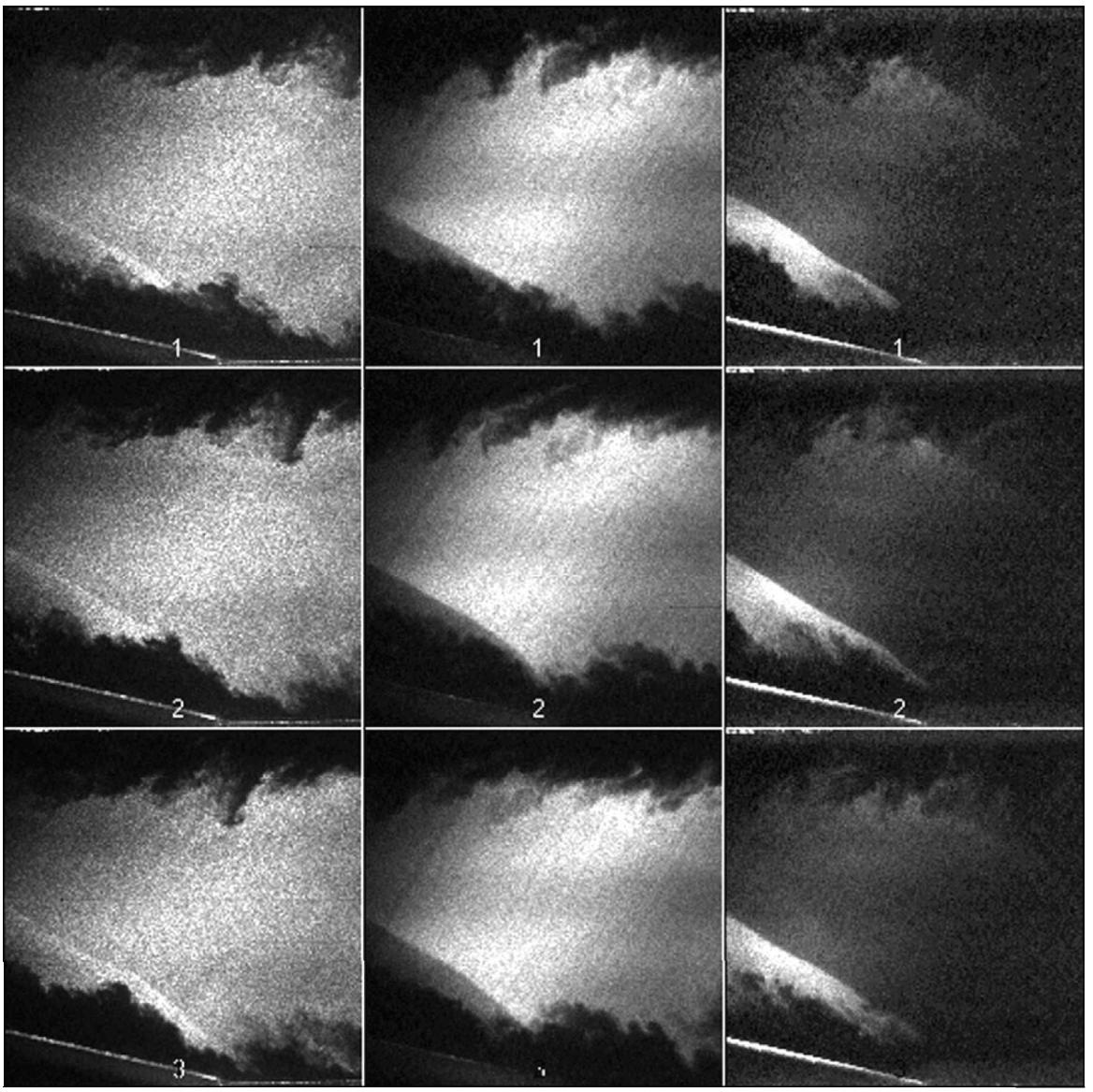

Fig. 13 Comparison of filtered and unfiltered side-view images. Flow from right to left with 4-θ s time interval between images: left column, unfiltered images; middle column, filtered to highlight high-speed flow; and right column, filtered to highlight low-speed flow.

the surface of the wedge is selectively attenuated, as illustrated in the middle column of Fig. 13. Alternatively, as shown in right column of Fig. 13, the scattering from the high-speed flow can also be suppressed by tuning the laser so that the Doppler-shifted-scattering coincides with the absorption line of iodine. The sequence of images in the right column also shows another weak oblique shock at the upper right corner. Without the filter the signal from the mean stream flow is so strong that it completely masks that shock-wave structure.

VIII. Conclusion and Future Work

A megahertz pulse-burst laser system has been developed and has been used for the visualization of shock-wave/boundary-layer interactions in a Mach 2.5 wind tunnel at a 0.5-MHz repetition rate.

The pulse-burst laser is capable of producing a programmable burst of from 1 to 99 pulses, with individual pulse duration from 10 to 100 ns and interpulse separation from 1 to 10 μs. A fundamental output energy (at 1.06 μm) of approximately 10 mJ has been achieved in each of 30 individual, 20-ns duration pulses. The second harmonic output was about 400 μJ per individual pulse.

Experimental results have shown that the laser has a narrow linewidth. The range of frequency tunability is about 1 cm^{-1} at 1.06 μm. The transmission through a 9.98-cm-long molecular iodine vapor filter (40°C side band, 80°C cell temperature) was measured to be 5×10^{-5}, which conforms well with model prediction. Consequently, the system can be used for FRS and other frequency or long coherence-length-related laser diagnostics, such as holography.

As an application of the megahertz pulse-burst laser system, the visualization of a Mach 2.5 flow over a 14-deg wedge shows the unsteadiness of a shock wave and its coupling to the structure of the incoming boundary layer.

We are now building a second-generation high-power pulse-burst laser system. Average single-pulse fundamental and second harmonic energy on the order of 100 and 25 mJ have been achieved, respectively. The new pulse-burst imaging system will be used for imaging in the plasma propulsion facility in the Electric Propulsion and Plasma Diagnostics Laboratory.

Acknowledgments

The authors wish to acknowledge Jay H. Grinstead and Philip Howard for their assistance in the Mach 2.5 imaging measurement. We would also like to thank A. J. Smits for the helpful discussion in the shock-wave/boundary-layer interaction and Princeton Scientific Instruments, Inc., for providing the megahertz-framing-rate CCD camera. The pulse-burst laser system has been developed with support from two grants from the U.S. Air Force Office of Scientific Research, Julian Tishkoff (University Research Initiative)

and Leonidas Sakell (External Aerodynamics), Technical Monitors. Money was also provided by NASA Phase 1 Project Grant NASA-97090 and the state-sponsored New Jersey Center for Opto-Electronics. The second-generation pulse-burst laser is supported by the Air Force Office of Scientific Research (Grant F49620-97-1-0373) as part of a joint Department of Defense University Research Initiative Program with the Princeton Electric Propulsion group. The CCD framing camera has been developed by Princeton Scientific Instruments, Inc., under Small Business Innovative Research grants from U.S. Office of Naval Research with Edwin Rood as Technical Monitor and the U.S. Air Force, Wright Laboratories, with Charles Tyler as Technical Monitor.

References

[1]Kyachoff, G., Seitzman, J., and Hanson, R. K., "Instantaneous Temperature Field Measurements Using Planar Laser-Induced Fluorescence," *Optics Letters*, Vol. 10, No. 9, 1985, pp. 439–441.

[2]Miles, R. B., and Lempert, W. R., "Two-Dimensional Measurement of Density, Velocity, and Temperature in Turbulent High-Speed Air Flows by UV Rayleigh Scattering," *Applied Physics*, Vol. B51, No. 1, 1990, pp. 1–7.

[3]Cheng, T. S., Wehrmeyer, J. A., and Pitz, R. W., "Simultaneous Temperature and Multispecies Measurement in a Lifted Hydrogen Diffusion Flame," *Combustion and Flame*, Vol. 91, No. 3/4, 1992, pp. 323–345.

[4]Wagner, J. W., Deaton, J. B., and Spicer, J. B., "Generation of Ultrasound by Repetitively Q-Switching a Pulsed Nd:YAG Laser," *Applied Optics*, Vol. 27, No. 22, 1988, pp. 4696–4700.

[5]Ruff, G. A., Bernal, L. P., and Faeth, G. M., "High Speed In-Line Holocinematography for Dispersed-Phase Dynamics," *Applied Optics*, Vol. 29, No. 31, 1990, pp. 4544–4546.

[6]Huntley, J. M., "High-Speed Laser Speckle Photography. Part 1: Repetitively Q-Switched Ruby Laser Light Source," *Optical Engineering*, Vol. 33, No. 5, 1994, pp. 1692–1699.

[7]Grace, J. M., Nebolsine, P. E., and Goldey, C. L., "Repetitively Pulsed Ruby Lasers as Light Sources for High-Speed Photography," *Optical Engineering*, Vol. 37, No. 8, 1998, pp. 2205–2212.

[8]Forkey, J. N., Finkelstein, N. D., Lempert, W. R., and Miles, R. B., "Demonstration and Characterization of Filtered Rayleigh Scattering for Planar Velocity Measurements," *AIAA Journal*, Vol. 34, No. 3, 1996, pp. 442–448.

[9]Forkey, J. N., Lempert, W. R., and Miles, R. B., "Corrected and Calibrated I_2 Absorption Model at Frequency Doubled Nd:YAG Laser Wavelengths," *Applied Optics*, Vol. 36, No. 27, 1997, pp. 6729–6738.

[10]Frantz, L. M., and Nodvik, J. S., "Theory of Pulse Propagation in a Laser Amplifier," *Journal of Applied Physics*, Vol. 34, No. 8, 1963, pp. 2346–2349.

[11]Lowdermilk, W. H., and Murry, J. E., "The Multipass Amplifier: Theory and Numerical Analysis," *Journal of Applied Physics*, Vol. 51, No. 5, 1980, pp. 2436–2444.

[12]Forkey, J. N., Lempert, W. R., and Miles, R. B., "Observation of a 100-MHz Frequency Variation Across the Output of a Frequency-Doubled Injection-Seeded Unstable-Resonator Q-Switched Nd:YAG Lasers," *Optics Letters*, Vol. 22, No. 4, 1997, pp. 230–232.

[13]Kosonocky, W. F., Yang, G., Ye, C., Kabra, R. K., Lowrance, J. L., Mastrocola, V., Shallcross, F. V., and Patel, V., "360*360 Element, Very High Framing Rate, Burst Image Sensor," 1996 IEEE International Solid-State Circuits Conf., San Francisco, Feb. 1996.

[14]Erbland, P. J., Baumgartner, M. L., Etz, M. R., Yalin, A., and Miles, R. B., "Development of Planar Diagnostics for Imaging Mach 8 Flowfields Using Carbon Dioxide and Sodium Seeding," AIAA Paper 97-0154, 1997.

[15]Smith, M. W., and Smits, A. J., "Visualization of the Structure of Supersonic Turbulent Boundary Layers," *Experiments in Fluids*, Vol. 18, No. 4, 1995, pp. 288–302.

R. P. Lucht
Associate Editor